International Journal of Nanomedicine

Dovepress
open access to scientific and medical research

Open Access Full Text Article

ORIGINAL RESEARCH

Cobalt-Doped Mesoporous Silica Coated Magnetic Nanoparticles Promoting Accelerated Bone Healing in Distraction Osteogenesis

Haoyu Zhao[1,*], Yachao Jia[1,*], Feng Wang[1], Yimin Chai[1], Chunfu Zhang[2], Jia Xu[1], Qinglin Kang[1]

[1]Shanghai Sixth People's Hospital Affiliated to Shanghai Jiao Tong University School of Medicine, Department of Orthopedic Surgery, Shanghai, People's Republic of China; [2]Shanghai Jiao Tong University, School of Biomedical Engineering, Shanghai, People's Republic of China

*These authors contributed equally to this work

Correspondence: Jia Xu; Qinglin Kang, Email xujia0117@126.com; orthokang@163.com

Introduction: Large bone abnormalities are commonly treated using distraction osteogenesis (DO), but it is not suitable for a long-term application; therefore, there is an urgent need for adjuvant therapy that can accelerate bone repair.

Methods: We have synthesized mesoporous silica-coated magnetic nanoparticles doped with cobalt ions (Co-MMSNs) and assessed their capacity to quicken bone regrowth in a mouse model of DO. Furthermore, local injection of the Co-MMSNs significantly accelerated bone healing in DO, as demonstrated by X-ray imaging, micro-CT, mechanical tests, histological evaluation, and immunochemical analysis.

Results: In vitro, the Co-MMSNs exhibited good biocompatibility and induced angiogenic gene expression and osteogenic development in bone mesenchymal stem cells. And the Co-MMSNs can promote bone regeneration in a rat DO model.

Discussion: This study demonstrated the significant potential of Co-MMSNs to shorten the DO treatment duration and effectively reduce the incidence of complications.

Keywords: mesoporous silica-coated magnetic nanoparticles, mesenchymal stem cells, large bone defects, distraction osteogenesis, bone regeneration

Introduction

Distraction osteogenesis (DO) is a common orthopaedic technique widely used for large bone defects and congenital or acquired osseous deformities.[1] The DO procedure consists of three sequential phases: the latency phase after osteotomy, the distraction phase to distract the bone ends using a distractor, and the consolidation phase to achieve new bone mineralisation and remodelling.[2] The advantage of DO, compared with other techniques used for bone defect reconstruction, is that it does not require bone tissue transplantation.[3] However, it should not be disregarded that DO requires a prolonged consolidation phase, which may lead to a high incidence of complications, such as stiffness of joints, nonunion, pin-track infection, and angular deformities.[4] Therefore, shortening the treatment duration and improving the treatment outcomes of DO are of great significance in clinical practice.

Recently, mesoporous silica nanoparticles (MSNs) have attracted considerable attention as a new generation of inorganic platforms for biomedical applications.[5,6] MSNs have unique properties, such as tunable particle size, stable and rigid frameworks, uniform and tunable pore size, high surface areas, large pore volumes, two functional surfaces, and a unique porous structure. MSNs are considered excellent candidates for drug delivery and targeting treatment.[7] Moreover, mesoporous silica-coated magnetic nanoparticles (M-MSNs) with a magnetic nanocrystal core encapsulated by a mesoporous silica shell possess the dual properties of mesoporous silica nanoparticles and magnetic nanoparticles, which are beneficial for bone regeneration. Experiments based on silicate (Si) scaffolds have been tested in animal models for bone regeneration, and Si ions are presumed to exert a bone-promoting effect, suggesting that mesoporous

Received: 14 December 2022
Accepted: 4 April 2023
Published: 8 May 2023

silica-coated magnetic nanoparticles can stimulate osteogenic differentiation of mesenchymal stem cells (MSCs) by releasing Si ions.[8] Besides, magnetic nanoparticles are universally used for tracking cells including MSCs.[9] Recent studies have also shown that these nanoparticles can promote the differentiation of MSCs into osteoblasts and accelerate the bone formation and consolidation during DO.[10,11] Therefore, M-MSNs may be considered an ideal candidate for inducing bone regeneration.

Many researchers have attempted to attach extra functionalities to M-MSNs by doping M-MSNs with metal ions such as Au, Zn, and Ti.[12–14] Cobalt (Co), usually considered a toxic element, has been reported to possess the angiogenesis-promoting property at concentrations below its toxic level.[15] This function involves the vascular endothelial-derived growth factor (VEGF), fibroblast growth factor (FGF), and hypoxia-inducible factor 1 (HIF-1) pathways.[16,17] At higher concentrations, Co2 + ions can reduce osteoclast cell numbers and resorption activity in vivo.[18] Co2+ ions affect the bone mesenchymal stem cells (BMSCs) through various pathways such as mediating the expression of transforming growth factor-beta (TGF-β) and genes associated with HIF-1 signalling.[18,19] Therefore, we speculated that Co-doped M-MSNs (Co-MMSNs) may exert a synergistic effect on osteogenic activity during DO and accelerate bone formation.

In the present study, we have assessed the therapeutic potential of Co-MMSNs in DO. We first evaluated the viability and pro-osteogenesis effect of Co-MMSNs on MSCs in vitro. The bone-regenerating capacity of the M-MSNs during DO in a rat tibial model was determined in vivo. Furthermore, the involvement of angiogenesis markers has been detected in vitro and in vivo.

Materials and Methods

Synthesis of Co-MMSNs

All the chemicals were purchased from Sinopharm (Shanghai, China) unless indicated otherwise. Cobalt-doped magnetite nanoparticles were prepared according to the method of a previous report.[20] Briefly, 2 mmol of Fe(acac)3, 1 mmol of Co(acac)2, 6 mmol of oleylamine, 6 mmol of oleic acid, and 10 mmol of 1.2-hexadecane-diol were dissolved in 20 mL of benzyl ether. The mixture was magnetically stirred, heated to 200 °C for 2 h using a nitrogen blanket, and refluxed at 300 °C for 1 h. The product was precipitated with ethanol and finally dispersed in hexane. To synthesize the mesoporous silica-coated magnetic nanoparticles, 0.6 mg of Co-doped Fe3O4 was dispersed in 0.74 mL of chloroform and mixed with 10 mL of hexadecyl trimethyl ammonium bromide aqueous solution (CTAB, 15 mg/mL). Stirring resulted in a uniform oil-in-water microemulsion, which was transferred into 45 mL of water with 2 mL of NaOH (2 M) and heated at 70 °C for 10 min. Subsequently, tetraethoxysilane (0.5 mL) and ethyl acetate (2 mL) were added dropwise and the reaction was allowed to proceed for 3 h. The resultant products were retrieved by centrifugation and the template was removed to generate mesopores by an extraction procedure using acetone as the solvent. The final product is designated as Co-MMSNs.

Characterisation of Co-MMSNs

The diameter, morphology, and microstructural characteristics of the Co-MMSNs were tested using transmission electron microscopy (TEM) (JEM 2010, Japan) at an acceleration voltage of 200 kV. N2 adsorption-desorption experiments were performed at 77 K to obtain the isotherm and mesopore size distribution of the Co-MMSNs using a Micromeritics instrument (ASAP 2010, Micromeritics, USA). The zeta potential was measured to determine the surface charges of the Co-MMSNs (Zetasizer Nano series, Nano ZS90, UK). Both nanoparticles were gently washed twice with phosphate-buffered saline (PBS; HyClone, USA) solution before the experiment.

Cell Culture

MSCs were collected from bone marrow as previously reported. In summary, cells were grown at 37 °C with 5% CO2 in alpha-modified Eagle's medium (α-MEM, Invitrogen) supplemented with 10% fetal bovine serum (FBS, Gibco) and 1% penicillin/streptomycin (Gibco, USA). In these studies, we used rBMSCs from passages three to six.

Cell Proliferation

Cell proliferation was assessed using Cell Counting Kit-8 (CCK-8; Dojindo Molecular Technologies, Inc., Japan). rBMSCs (5 × 103 cells/well) were seeded in 96-well plates. After culturing with serial concentrations of the Co-MMSNs for 6 h, 12 h, and

24 h, CCK-8 solution was added to each plate and then the plates were incubated for another 2 h. After this, the optical density (OD) values were measured at 450 nm using a microplate reader (Bio-Rad, USA).

Osteogenic Differentiation

Cells were seeded in 24-well plates at a density of 5×104 cells per well and then treated with osteogenic induction medium (OIM; 20 mM β-glycerophosphate, 1 nM dexamethasone, and 50 μM L-ascorbic acid-2- phosphate in the complete medium; Sigma-Aldrich) containing serial concentrations of Co-MMSNs. Every 2 days, the medium was replaced with fresh medium. After 7 days, alkaline phosphatase (ALP) staining and activity assays were performed according to the manufacturer's instructions (KeyGEN, China). After 21 days of treatment, the cells were fixed with 4% (v/v) formaldehyde and stained with 40 mM alizarin red S (ARS) (pH 4.2) for 30 min at room temperature. The cells were monitored and photographed using a microscope (Axiovert 40; Zeiss, Germany) to detect the production of mineralised matrix nodules.

Enzyme-Linked Immunosorbent Assay (ELISA)

The supernatant was collected from rBMSCs grown for 24 h and 72 h with 10 ug/mL M-MSNs and Co-MMSNs. The M-MSNs were synthesized as previously reported.[21] The released VEGF was measured using an ELISA kit (Uscnlife, China), according to the manufacturer's instructions. Each experiment was conducted in triplicates. Correlation with a standard curve was used to quantify the VEGF concentration, and the results were represented as the quantity (pg) of VEGF in each millilitre of supernatant.

RNA Isolation and Quantitative Real-Time Polymerase Chain Reaction (qRT-PCR) Analysis

rBMSCs were seeded in a 6-well plate (1 × 105 cells/well) and cultured overnight. They were subsequently treated with Co-MMSNs (final concentration 10 μg/mL) for 7 days, total RNA was extracted using a tissue RNA Purification Kit (EZBioscience, USA), and the RNA was reverse-transcribed using the Reverse Transcription Kit (EZBioscience), according to the manufacturer's instructions. All q-PCR reactions were performed in triplicate using a 10 mL reaction system (Takara, Japan), including cDNA, primers, and SYBR-green mix. The following protocol was used to perform PCR: a 10-minute denaturation stage at 95 °C followed by 40 cycles of 15s at 95 °C and 60s at 60 °C. Table 1 contains information on the gene-specific primers. The 2-ΔΔCT method was used to assess the relative quantification of gene expression.

Animal Surgery and Treatment

All experimental protocols were approved by the Animal Welfare Ethics Committee of the Shanghai Jiao Tong University and conducted in accordance with the "Guiding Principles in the Care and Use of Animals" (China) Affiliated Sixth People's Hospital. Thirty-two adult male SD rats (350–400 g) were randomly allocated to either the control (n = 16) or Co-MMSNs (n = 16) groups. After anaesthesia and exposure, a transverse osteotomy was performed at the midshaft of the right tibia to construct the DO model. Proximal and distal sections of the tibia were fixed using a specially developed monoliteral external fixator (Xinzhong Company, China). Subsequently, surgical incisions were closed layer-by-layer. The periosteum was maintained as much as possible during this process. Three stages comprised the DO procedure: a 5-day latency phase; a 10-day progressive lengthening phase (0.5 mm/d in two increments, every 12 h); and a 4-week consolidation phase. At 0 and 2 weeks after distraction, rats in the two groups received local injections of PBS (100 L) or Co-MMSNs (100 g in 100 L PBS) into the distraction gaps.

Table 1 Primer Sequences

Gene	Forward (5'–3')	Reverse (5'–3')
ALP	CCGCAGGATGTGAACTACT	GGTACTGACGGAAGAAGGG
Runx2	ACTTCCTGTGCTCGGTGCT	GACGGTTATGGTCAAGGTGAA
OCN	CAGACAAGTCCCACACAGCA	CCAGCAGAGTGAGCAGAGAGA

Digital Radiographs and Micro-Computed Tomography (Micro-CT)

Weekly radiographs focusing on the distraction gap were obtained under anaesthesia. After 2 and 4 weeks of consolidation, distracted tibia specimens were collected and subjected to an 18-m resolution micro-CT scan (SKYSCAN 1176, Bruker, Kontich, Belgium). We conducted three-dimensional (3D) reconstructions of the regenerated callus and examined metrics after consolidation for 4 weeks, including bone volume/tissue volume (BV/TV) and bone mineral density (BMD).

Biomechanical Testing

After consolidation for 4 weeks, the mechanical characteristics of the fresh tibial specimens were determined using a three-point bending device (n = 6 per group) (Instron, Norwood, MA, USA). The anterior-posterior tibia samples were loaded at a rate of 1 mm/min until failure. We examined the ultimate stress and energy required to result in the failure of extended tibias.

Histological and Immunohistochemistry Staining

After 48 h of fixation in 4% paraformaldehyde, the tibia specimens were decalcified for 4 weeks in 10% ethylenediaminetetraacetic acid solution and embedded in paraffin. In the sagittal plane, thin slices (5 μm) were cut along the long axis of each specimen for subsequent haematoxylin-eosin (HE) and Masson's trichrome staining. Primary antibodies against rabbit CD31 (Abcam, 1:100) and osteocalcin (OCN; Santa Cruz Biotechnology, 1:100) were used for immunohistochemical staining, and this was performed overnight at 4 °C. Then, a horseradish peroxidase-streptavidin detection method was used (Dako, USA), followed by haematoxylin counterstaining.

Statistical Analysis

All data are presented as mean ± standard deviation. Student's *t*-test was used to examine differences in study variables between two groups, and one-way ANOVA followed by Tukey's post hoc test was used to investigate differences between three or more groups, using GraphPad Prism 5. $P < 0.05$ was regarded as statistically significant.

Results

The Morphology and Mesostructure of the Co-MMSNs

According to the low-magnification TEM study, the spheres were typically 60–100 nm in diameter (Figure 1A). The TEM scans revealed the dispersity and shape of the Co-MMSNs (Figure 1B). As shown in Figure 1C, the Co-MMSNs exhibited a conventional type-IV N2 adsorption-desorption isotherm with well-defined steps at 0.2–0.4 relative pressure (p/p0). This indicates that the Co-MMSNs were uniformly mesoporous with a small pore size distribution, which is corroborated by the findings shown in Figure 1D.

The Effect of Co-MMSNs on Cell Viability

rBMSCs were cultured with different concentrations of Co-MMSNs in αMEM (5, 10, 25, and 50 μg/mL) for 6 h, 12 h, and 24 h. According to the results of the CCK8 assay (Figure 2), the Co-MMSNs at different concentrations showed no obvious cytotoxicity compared to the blank control.

The ALP and ARS Staining of rBMSCs Cultured with Co-MMSNs

As shown in Figure 3A, ALP staining was stronger after Co-MMSN treatment. More calcium deposits were observed in the Co-MMSN group than in the control group (Figure 3B). Furthermore, the quantitative results of the ALP activity and ARS staining showed that Co-MMSN treatment remarkably increased ALP activity and calcium mineral deposition in a dose-dependent manner (Figure 3C and D), with Co-MMSNs at 10 μg/mL showing the best pro-osteogenesis effect.

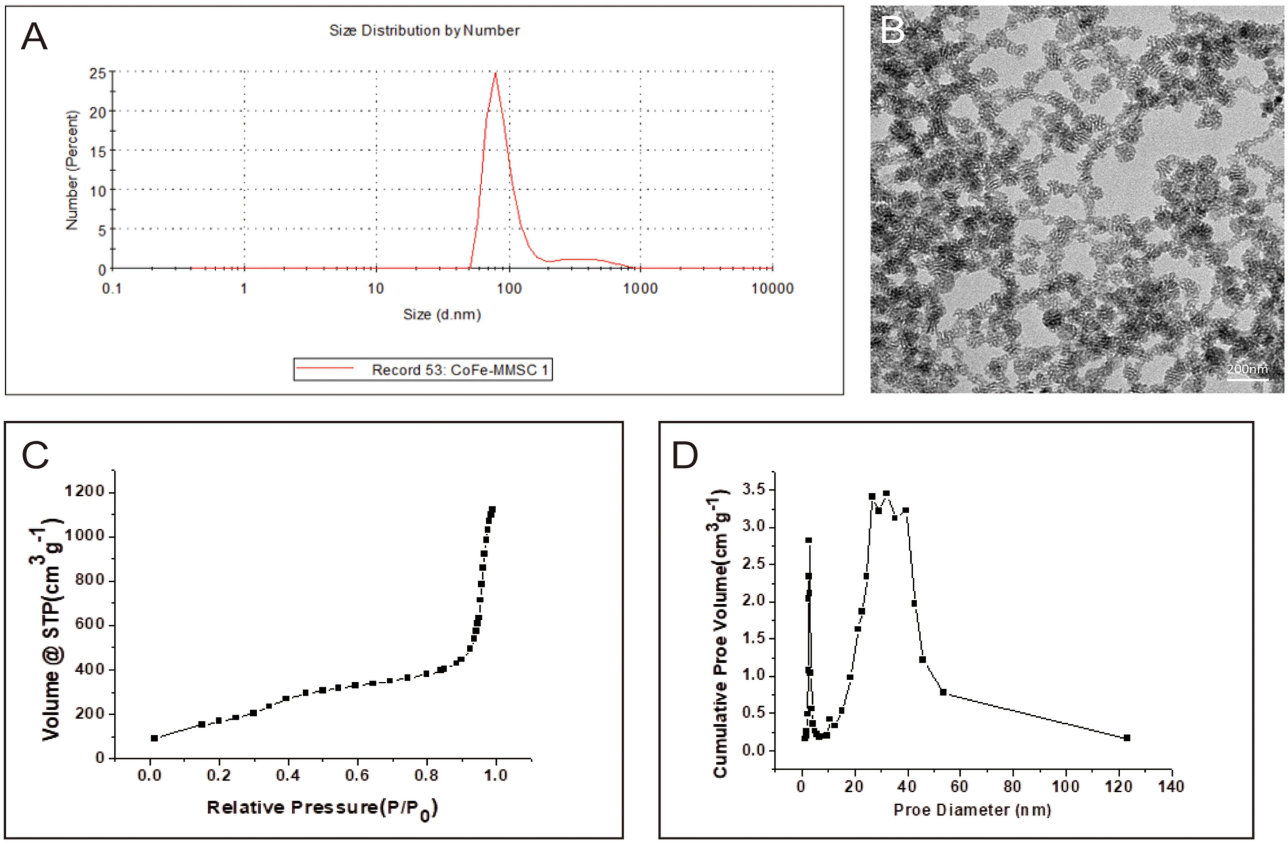

Figure 1 (**A**) Sphere size from the low-magnification TEM analysis, (**B**) Representative TEM image of Co-MMSNs. (**C**) N2 adsorption–desorption isotherm of Co-MMSNs and (**D**) Mesopore pore size distribution.

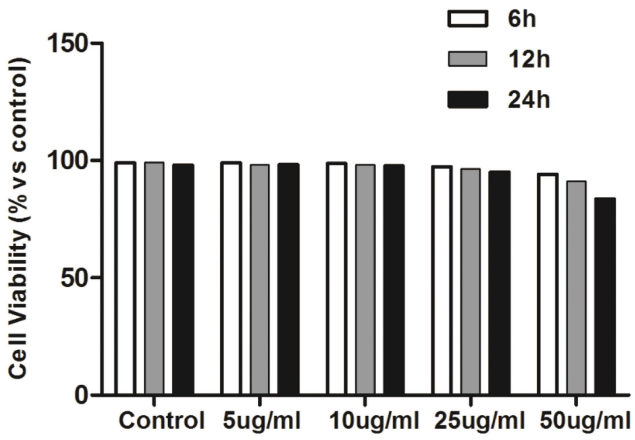

Figure 2 The effect of Co-MMSNs on cell viability.

VEGF Secretion by rBMSCs Cultured with Co-MMSNs

VEGF secretion by rBMSCs showed no clear difference between the M-MSN group and the blank control (Figure 4). However, the concentration of VEGF secreted from the rBMSCs cultured with Co-MMSNs was clearly higher than that from other groups, especially at 72 h.

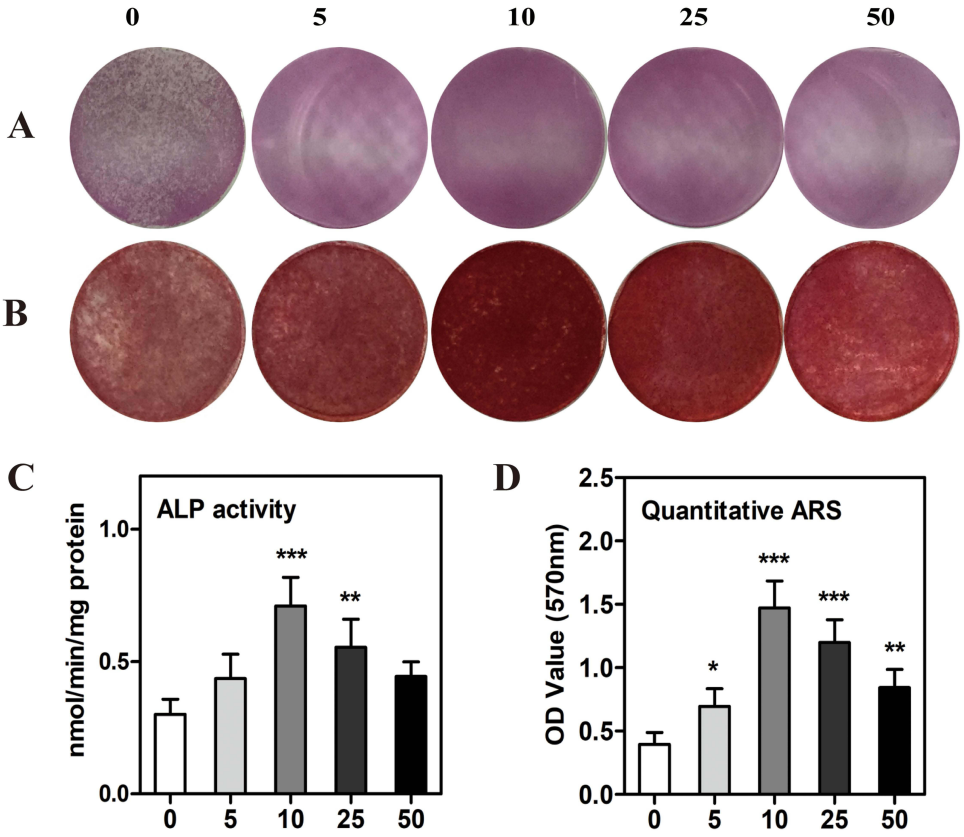

Figure 3 Co-MMSN enhanced the osteogenic differentiation of rBMSCs. (**A and B**) Typical ALP staining at day 7 for ALP activity and ARS staining at day 21 for calcium mineral deposition in rBMSCs treated with PBS or Co-MMSN with different concentrations (0, 5, 10, 25, 50 ug/mL). (**C** and **D**) Quantitative analysis of ALP activity and calcium mineral deposition. The **P < 0.05, **P < 0.01, ***P < 0.001*.

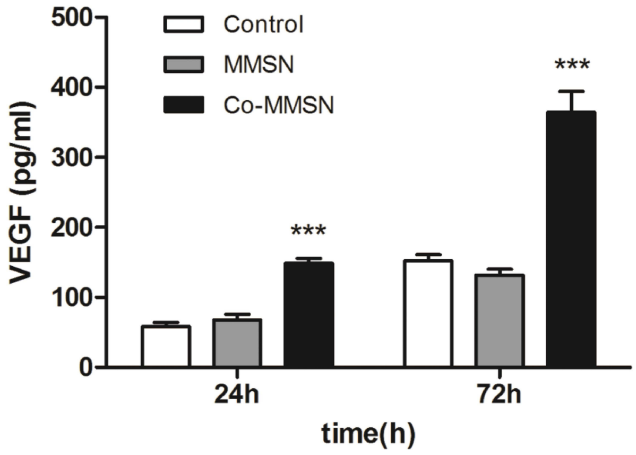

Figure 4 The effect of Co-MMSN on VEGF secretion of rBMSCs after cultured for 24h and 72h. The ****P < 0.001*.

Expression of the Bone-Related Genes of rBMSCs Cultured with Co-MMSNs

The qRT-PCR analysis showed that OCN, ALP, and Runx2 were upregulated by the Co-MMSNs when compared with the control group, which indicated that the Co-MMSNs enhanced the osteogenic differentiation of rBMSCs (Figure 5A–C).

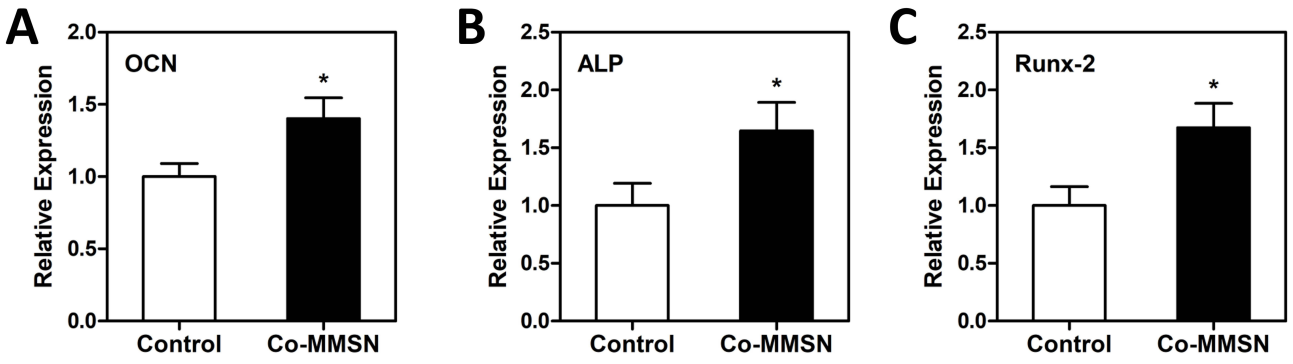

Figure 5 The effect of Co-MMSN on bone-related gene expression of rBMSCs after cultured for 3 days. (**A**) OCN, (**B**) ALP and (**C**) RUNX2. The *$P < 0.05$.

The Effect of Co-MMSNs on New Bone Formation During DO in Older Rats

All of the rats survived the DO procedure without complications. Little callus was observed in the distraction gaps immediately after the distraction phase in both groups. A new callus formed from the proximal and distal osteotomy ends at the centre of the distraction gaps. Mineralised callus formation increased over time in both groups. More calluses were observed in the Co-MMSN group than in the PBS group at each time point (0, 1, 2, and 4 weeks). Typical radiographs from Co-MMSN-treated rats and PBS-treated rats at 0, 1, 2, and 4 weeks after distraction are shown in Figure 6. Bone regeneration was further quantified using micro-CT scans after consolidation for 2 and 4 weeks. Representative 3D reconstructions of distracted tibias are shown in Figure 7A. Both the BV/TV and BMD values in the Co-MMSN group were significantly higher than those in the PBS group at 4 weeks ($P < 0.01$) (Figure 7B and C).

Mechanical Test

The bone mechanical property test results were consistent with the imaging results. Both the values of ultimate load and energy to failure in the Co-MMSN group showed significant improvement when compared with those in the control group ($P < 0.05$) (Figure 8A and B). It was proven that the bone's mechanical competence in the Co-MMSN group was better than that in the control group at the macroscale.

Histological and Immunohistochemical Analyses

The results of HE and Masson's trichrome staining of the distraction regeneration demonstrated that the distraction gaps consisted of various amounts of fibrous tissues, cartilaginous tissues, and newly formed calluses. A new callus was formed from the proximal and distal cross ends to the centre of the distraction gaps. The middle distraction gaps in the PBS groups were linked mainly by fibrous and cartilaginous tissues, whereas the distraction gaps in the Co-MMSN group were bridged by newly formed calluses (Figure 9). OCN is a protein secreted by mature osteocytes and can be used as a marker of mature osteocytes. CD31 is a target to detect the formation and location of blood vessels. By immunohistochemical technique, we mapped the location of these two proteins in tibial specimens after 4 weeks of distraction osteogenesis (Figure 10A and B). By quantitative analysis, it was found that the number of OCN-positive cells in the bone space formed by Co-MMSN was significantly higher than that of the control group, and the expression of CD31 was also higher (Figure 10C and D).

Discussion

In previous studies, we determined the effects of M-MSNs on osteogenic differentiation of MSCs and assessed their potential to accelerate bone regeneration during DO in a rat tibial model.[11] Here, we have successfully synthesised new M-MSNs doped with cobalt ions (Co-MMSNs) which have exhibited the dual properties of nanoparticles and Co2+ ions. We have then verified the stimulatory effect of the Co-MMSNs on osteogenic differentiation in vivo and in vitro.

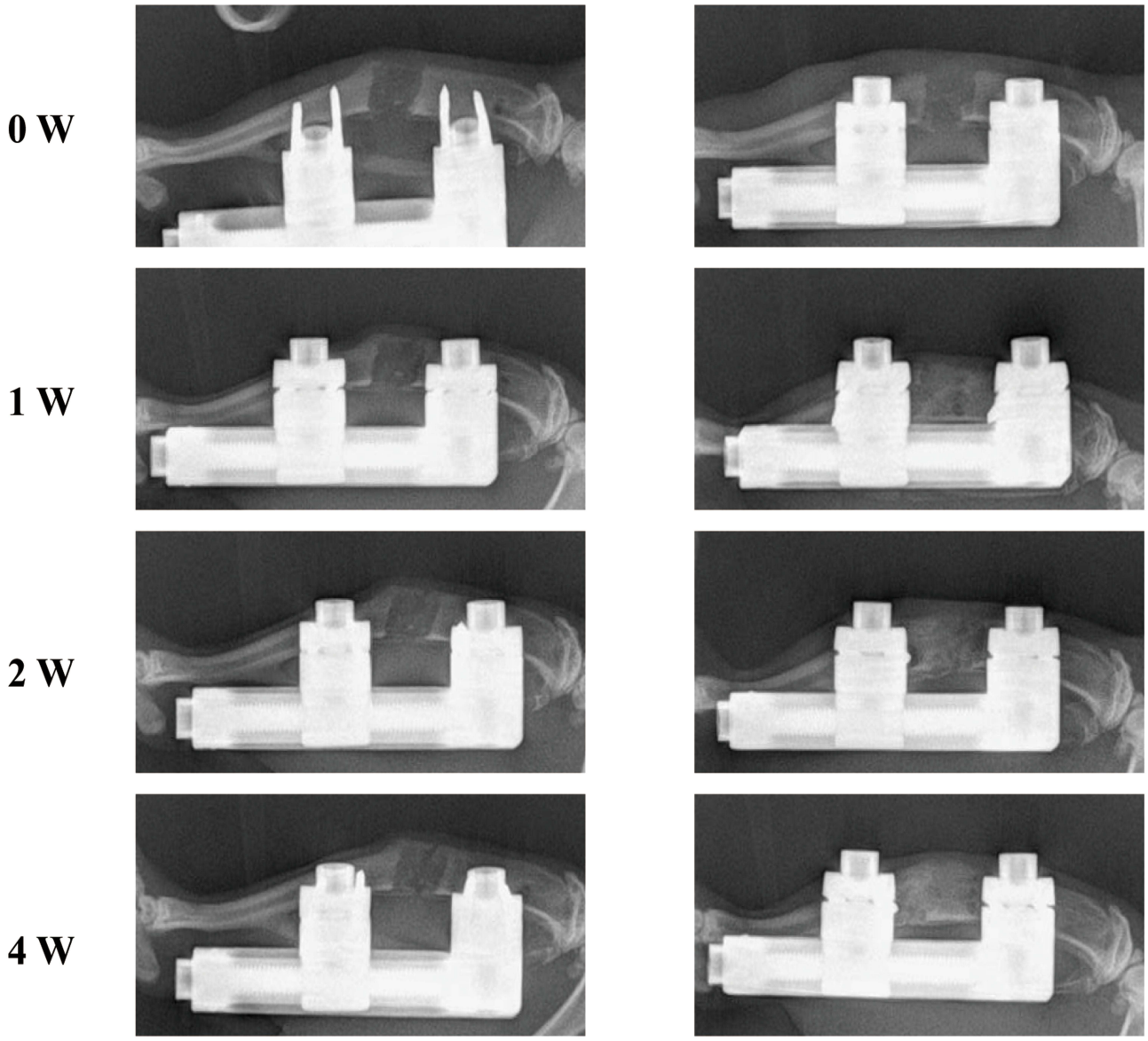

Figure 6 X-ray images of the distraction regenerates from the PBS and Co-MMSNs group after consolidation for 0, 1, 2 and 4 weeks.

The cytotoxicity assays demonstrated good biocompatibility and low toxicity of Co-MMSNs. Furthermore, the biological experiments revealed that M-MSNs can promote the osteogenic differentiation of the rBMSCs. It is well documented that ALP is an early marker of osteoblasts and promotes new bone formation by hydrolysing pyrophosphate into phosphate, which then reacts with calcium to form hydroxyapatite and stimulate matrix mineralisation.[22] In addition, OCN, the most abundant non-collagenous bone matrix protein, is a specific marker of mature osteoblasts that can regulate the gene expression of osteogenic markers including Runx2, alkaline phosphatases, osteonectin, and type I collagen.[23,24] Runx2 is an essential transcription factor for osteoblast differentiation in MSCs.[25] It can positively regulate many osteoblast-specific genes, such as Col-I and OCN (early and late osteoblastic markers), and it can effectively improve the osteogenic potential of MSCs.[26] In our experiments, Co-MMSNs have been shown to fully enhance the osteogenic differentiation of MSCs in vitro by increasing ALP activity, matrix mineralisation, and upregulating the expression levels of ALP, OCN, and Runx2 osteogenic genes. In addition, the increase in extracellular VEGF concentration indicated that the Co-MMSNs stimulated the angiogenic activity of osteoblasts.

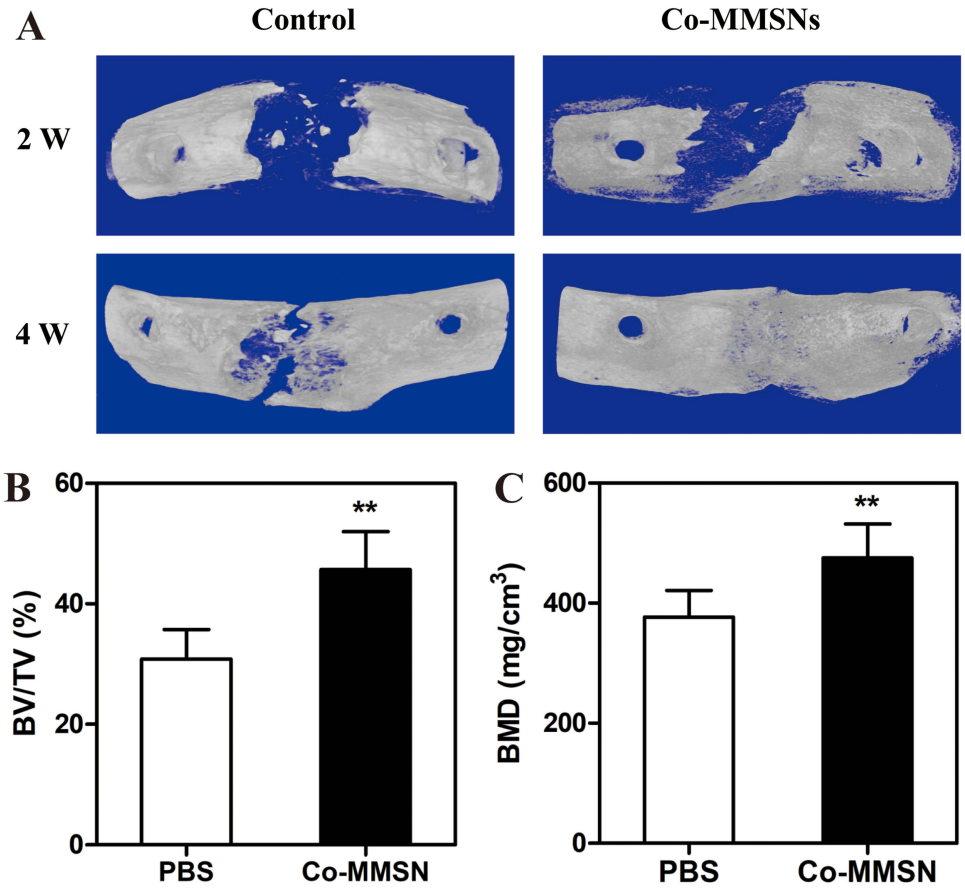

Figure 7 Co-MMSN accelerated new bone formation during distraction osteogenesis in older rats. (**A**) Representative 3D micro-CT images of the distraction regenerates after consolidation for 2 and 4 weeks indicated more mineralized callus in the Co-MMSN group. (**B** and **C**) Quantitative analysis of the micro-CT data demonstrated that Co-MMSN significantly increased the values of BV/TV and BMD after consolidation for 4 weeks.

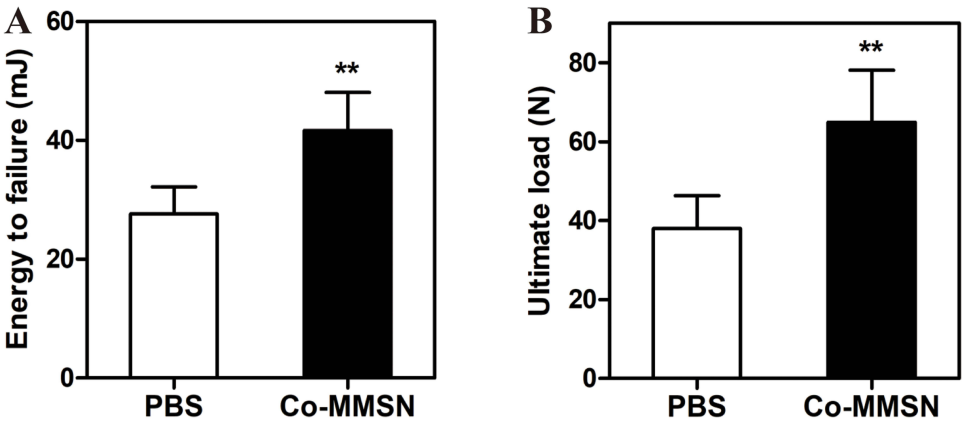

Figure 8 (**A** and **B**) Mechanical properties (energy to failure and ultimate load) of the distracted tibias after consolidation for 4 weeks. $^{**}P < 0.01$.

We have established a rat tibial DO model to further evaluate the effect of Co-MMSNs on bone regeneration. Weekly X-ray images and biweekly microscopic CT showed that local injection of Co-MMSNs into the distraction gap could efficiently promote new bone formation. At the same time, the results of ultimate load and energy to failure also confirmed that the quality of the callus was better in the Co-MMSN group. Histological observations were also consistent

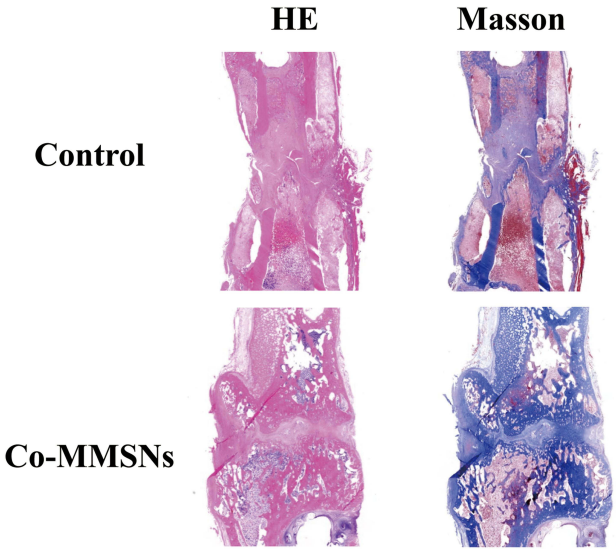

Figure 9 Representative histological staining of the middle distracted regenerates from two groups after consolidation for 4 weeks. The H&E and Masson's trisome staining showed newly formed callus in the Co-MMSN group, and fibrous and cartilaginous tissues in the PBS group.

with radiological results. Finally, the higher expression of OCN and CD31 in the distraction regeneration from the Co-MMSN group indicated enhanced osteogenic differentiation of the BMSCs and vessel restoration in vivo.

Although there has been no direct comparison of the bone-promoting ability of Co-MMSNs with other drugs or biological interventions previously reported, including cytokines, growth factors, and stem cells, we believe that Co-MMSNs may have some advantages in DO. Silica nanoparticles have high stability and good biocompatibility, unlike common drugs, which are usually limited by rapid clearance, uneven concentration distribution, and possible toxicity.[27] Meanwhile, silica nanoparticles do not suffer from immunogenicity issues and the risk of tumour formation, such as in stem cell therapies.[28]

Early research established that M-MSNs can promote bone regeneration during DO through the Wnt/β-catenin pathway.[11] The aim of the present study was to examine the osteogenic propensity of Co-MMSNs. We have discovered that Co-MMSNs enhanced the osteogenic differentiation of rBMSCs. Further, Co-MMSNs increased VEGF secretion by rBMSCs. Osteogenesis and angiogenesis are tightly coupled during DO.[29] The simultaneous promotion of osteogenesis and angiogenesis has a synergistic effect on bone regeneration. Therefore, by doping Co2 + ions on the surface of the M-MSNs, the regeneration process of DO was accelerated through the promotion of osteogenesis and angiogenesis. Thus, the potential of Co-MMSNs for bone regeneration has been demonstrated for the first time.

The major limitation of this study is that the mechanisms underlying osteogenesis and angiogenesis are not fully understood. Co-MMSNs have the dual properties of mesoporous silica nanoparticles and magnetic nanoparticles, and the Co2+ ions carried by the Co-MMSNs can promote both osteogenesis and angiogenesis. The complexity of the mechanics requires further investigation.

In conclusion, we have demonstrated the therapeutic potential of Co-MMSNs in enhancing bone regeneration in a rat tibial DO model. Co-MMSNs coated with mesoporous silica and doped with Co ions showed good biocompatibility in vitro and could significantly induce the osteogenic differentiation of rBMSCs. More importantly, the local injection of Co-MMSNs significantly accelerated the formation and consolidation of new bone during DO in rats. Given the excellent performance of Co-MMSNs in targeting and controlling drug delivery, these nanoparticles may have great potential for the clinical treatment of large bone defects.

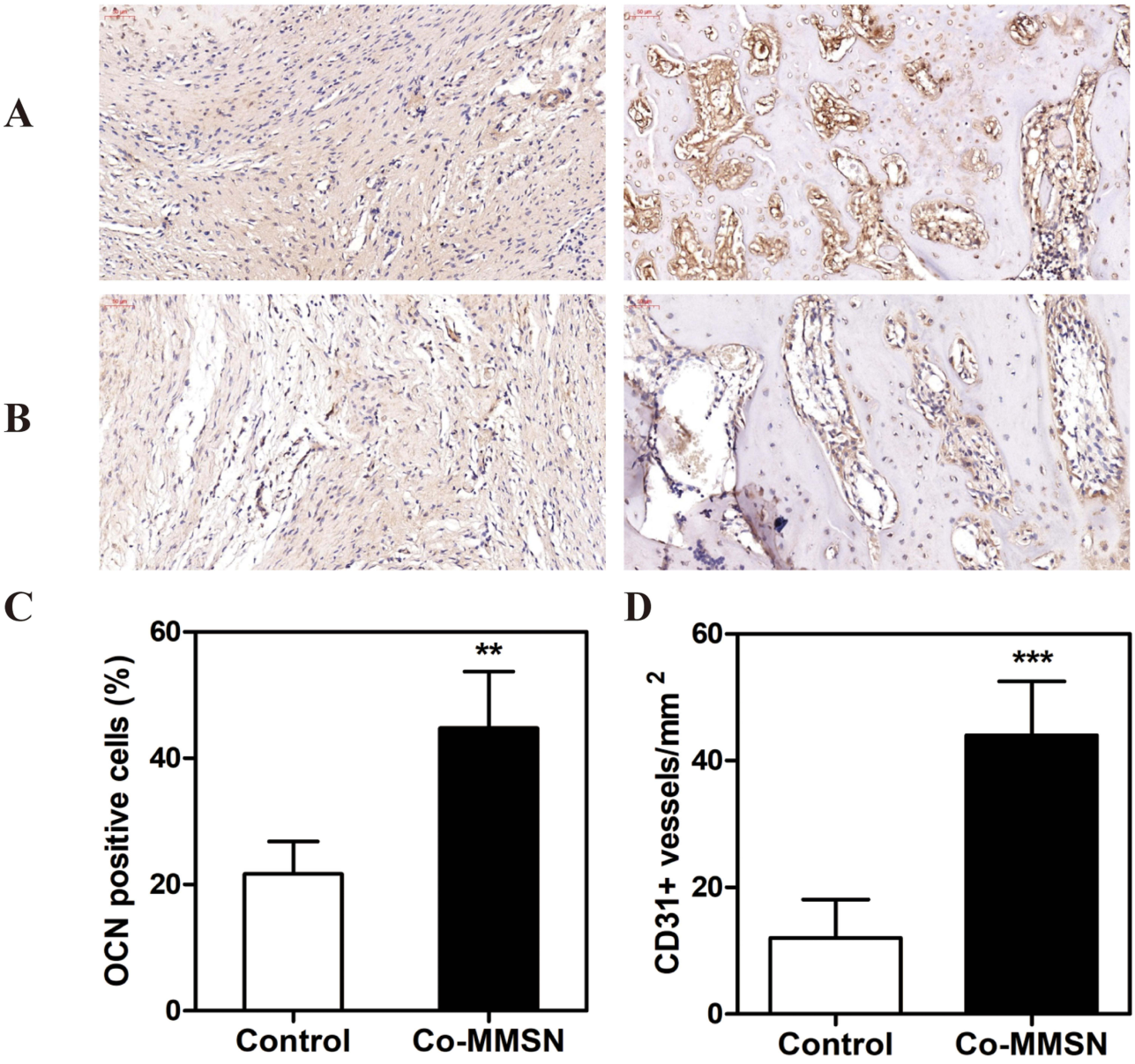

Figure 10 (**A** and **B**) Location of OCN and CD31 proteins in tibial specimens after 4 weeks of distraction osteogenesis. (**C** and **D**) Quantitative analysis of two proteins, OCN and CD31. ***P* < *0.01*.

Conclusion

This study demonstrates the important potential of co-MmsNs to promote bone regeneration during DO. The application of co-MMSNS can shorten the treatment time of DO and effectively reduce the incidence of complications.

Disclosure

The authors report no conflicts of interest in this work.

References

1. Alzahrani MM, Anam E, AlQahtani SM, Makhdom AM, Hamdy RC. Strategies of enhancing bone regenerate formation in distraction osteogenesis. *Connect Tissue Res*. 2018;59(1):1–11. doi:10.1080/03008207.2017.1288725
2. Li Y, Pan Q, Xu J, et al. Overview of methods for enhancing bone regeneration in distraction osteogenesis: potential roles of biometals. *J Orthop Translat*. 2021;27:110–118. doi:10.1016/j.jot.2020.11.008

3. Yang S, Wang N, Ma Y, Guo S, Guo S, Sun H. Immunomodulatory effects and mechanisms of distraction osteogenesis. *Int J Oral Sci*. 2022;14(1):4. doi:10.1038/s41368-021-00156-y
4. Kim HS, Lee YS, Jung JH, Shim JS. Complications of distraction osteogenesis in brachymetatarsia: comparison between the first and fourth brachymetatarsia. *Foot Ankle Surg*. 2019;25(2):113–118. doi:10.1016/j.fas.2017.09.004
5. Zhou Y, Quan G, Wu Q, et al. Mesoporous silica nanoparticles for drug and gene delivery. *Acta Pharm Sin B*. 2018;8(2):165–177. doi:10.1016/j.apsb.2018.01.007
6. Andrée L, Barata D, Sutthavas P, Habibovic P, van Rijt S. Guiding mesenchymal stem cell differentiation using mesoporous silica nanoparticle-based films. *Acta Bio*. 2019;96:557–567. doi:10.1016/j.actbio.2019.07.008
7. Slowing II, Vivero-Escoto JL, Wu CW, Lin VS. Mesoporous silica nanoparticles as controlled release drug delivery and gene transfection carriers. *Adv Drug Deliv Rev*. 2008;60(11):1278–1288. doi:10.1016/j.addr.2008.03.012
8. Guan J, Zhang J, Guo S, et al. Human urine-derived stem cells can be induced into osteogenic lineage by silicate bioceramics via activation of the Wnt/β-catenin signaling pathway. *Biomaterials*. 2015;55:1–11. doi:10.1016/j.biomaterials.2015.03.029
9. Zheng B, von See MP, Yu E, et al. Quantitative magnetic particle imaging monitors the transplantation, biodistribution, and clearance of stem cells in vivo. *Theranostics*. 2016;6(3):291–301. doi:10.7150/thno.13728
10. Wang Q, Chen B, Cao M, et al. Response of MAPK pathway to iron oxide nanoparticles in vitro treatment promotes osteogenic differentiation of hBMSCs. *Biomaterials*. 2016;86:11–20. doi:10.1016/j.biomaterials.2016.02.004
11. Jia Y, Zhang P, Sun Y, et al. Regeneration of large bone defects using mesoporous silica coated magnetic nanoparticles during distraction osteogenesis. *Nanomedicine*. 2019;21:102040. doi:10.1016/j.nano.2019.102040
12. Sha Z, Yang S, Fu L, et al. Manganese-doped gold core mesoporous silica particles as a nanoplatform for dual-modality imaging and chemo-chemodynamic combination osteosarcoma therapy. *Nanoscale*. 2021;13(9):5077–5093. doi:10.1039/D0NR09220G
13. Liu M, Sun X, Liao Z, et al. Zinc oxide end-capped Fe(3)O(4)@mSiO(2) core-shell nanocarriers as targeted and responsive drug delivery system for chemo-/ions synergistic therapeutics. *Drug Deliv*. 2019;26(1):732–743. doi:10.1080/10717544.2019.1642419
14. Sun G, Chang Y, Li S, et al. pH-responsive controlled release of antitumour-active polyoxometalate from mesoporous silica materials. *Dalton Trans*. 2009;23:4481–4487. doi:10.1039/b901133a
15. Bosch-Rué E, Díez-Tercero L, Rodríguez-González R, Bosch-Canals BM, Perez RA. Assessing the potential role of copper and cobalt in stimulating angiogenesis for tissue regeneration. *PLoS One*. 2021;16(10):e0259125. doi:10.1371/journal.pone.0259125
16. Solanki AK, Lali FV, Autefage H, et al. Bioactive glasses and electrospun composites that release cobalt to stimulate the HIF pathway for wound healing applications. *Biomater Res*. 2021;25(1):1. doi:10.1186/s40824-020-00202-6
17. Haddadi G, Abbaszadeh A, Mosleh-Shirazi MA, Okhovat MA, Salajeghe A, Ghorbani Z. Evaluation of the effect of hesperidin on vascular endothelial growth factor gene expression in rat skin animal models following cobalt-60 gamma irradiation. *J Cancer Res Ther*. 2018;14:S1098–s1104. doi:10.4103/0973-1482.202892
18. Shah KM, Dunning MJ, Gartland A, Wilkinson JM. Distinct concentration-dependent molecular pathways regulate bone cell responses to cobalt and chromium exposure from joint replacement prostheses. *Int J Mol Sci*. 2021;22:10. doi:10.3390/ijms22105225
19. Drynda S, Drynda A, Feuerstein B, Kekow J, Lohmann CH, Bertrand J. The effects of cobalt and chromium ions on transforming growth factor-beta patterns and mineralization in human osteoblast-like MG63 and SaOs-2 cells. *J Biomed Mater Res A*. 2018;106(8):2105–2115. doi:10.1002/jbm.a.36409
20. Sun S, Zeng H, Robinson DB, et al. Monodisperse MFe2O4 (M = Fe, Co, Mn) nanoparticles. *J Am Chem Soc*. 2004;126(1):273–279. doi:10.1021/ja0380852
21. Zhang J, Li X, Rosenholm JM, Gu HC. Synthesis and characterization of pore size-tunable magnetic mesoporous silica nanoparticles. *J Colloid Interface Sci*. 2011;361(1):16–24. doi:10.1016/j.jcis.2011.05.038
22. Harrison G, Shapiro IM, Golub EE. The phosphatidylinositol-glycolipid anchor on alkaline phosphatase facilitates mineralization initiation in vitro. *J Bone Miner Res*. 1995;10(4):568–573. doi:10.1002/jbmr.5650100409
23. Nakamura A, Dohi Y, Akahane M, et al. Osteocalcin secretion as an early marker of in vitro osteogenic differentiation of rat mesenchymal stem cells. *Tissue Eng Part C Methods*. 2009;15(2):169–180. doi:10.1089/ten.tec.2007.0334
24. Tsao YT, Huang YJ, Wu HH, Liu YA, Liu YS, Lee OK. Osteocalcin mediates biomineralization during osteogenic maturation in human mesenchymal stromal cells. *Int J Mol Sci*. 2017;18:1. doi:10.3390/ijms18010159
25. Ducy P, Zhang R, Geoffroy V, Ridall AL, Karsenty G. Osf2/Cbfa1: a transcriptional activator of osteoblast differentiation. *Cell*. 1997;89(5):747–754. doi:10.1016/S0092-8674(00)80257-3
26. Zhang X, Yang M, Lin L, et al. Runx2 overexpression enhances osteoblastic differentiation and mineralization in adipose--derived stem cells in vitro and in vivo. *Calcif Tissue Int*. 2006;79(3):169–178. doi:10.1007/s00223-006-0083-6
27. Makhdom AM, Hamdy RC. The role of growth factors on acceleration of bone regeneration during distraction osteogenesis. *Tissue Eng Part B Rev*. 2013;19(5):442–453. doi:10.1089/ten.teb.2012.0717
28. Herberts CA, Kwa MS, Hermsen HP. Risk factors in the development of stem cell therapy. *J Transl Med*. 2011;9:29. doi:10.1186/1479-5876-9-29
29. Hamushan M, Cai W, Zhang Y, et al. High-purity magnesium pin enhances bone consolidation in distraction osteogenesis model through activation of the VHL/HIF-1α/VEGF signaling. *J Biomater Appl*. 2020;35(2):224–236. doi:10.1177/0885328220928550